Square-Signal-Based Algorithm for Analog Lock-In Amplifiers

Javier Aguirre, Daniel García-Romeo, Nicolás Medrano, *Member, IEEE*, Belén Calvo, *Member, IEEE*, and Santiago Celma

***Abstract*—Dual-phase lock-in amplifiers (LIAs) are designed to extract information (amplitude and phase) from signals buried in high noise levels. In spite of their popularity, their use has been traditionally limited to input sinusoidal waves with symmetric power supplies. This paper presents an algorithm that enables single-supply analog LIAs to properly process input square waves. Formed by linear equations, its computational implementation is much simpler than that of the traditional sinusoidal algorithm. Moreover, applied to battery-operated microcontrolled systems where square signals can be generated by the embedded microcontroller, it presents intrinsic advantages such as simplicity, versatility, and reduction in power and size. Experimental results validate the proposed algorithm, confirming its enormous possibilities in sensing applications.**

***Index Terms*—Lock-in amplifier (LIA), noise rejection, phase-sensitive detection (PSD), sensor interfaces.**

I. Introduction

RECENT advances in portable sensing systems and smart sensor interfaces rendered monitoring of hostile environments, i.e., hitherto considered a formidable task, a distinct possibility. One of the main problems encountered by the measurement systems is the presence of electrical noise, whose sources are diverse but the result is always the same: contamination of sensor output signals. In extreme cases, when sensor output levels are very low compared to noise levels, relevant signal information will get completely buried in nondesired components. This phenomenon distorts the measurements leading to failure of the processing capability of the monitoring system, unless suitable improvements are effected in the signal processing methods.

An interesting possibility in this direction is the lock-in amplifier (LIA), which uses phase-sensitive detection (PSD) technique to take out the data signal at a specific reference frequency and reject noise signals at different frequencies without affecting the measurement significantly [1]–[4]. LIAs have become a popular laboratory measurement instrument by virtue of their versatility as a signal recovery system. Traditionally, they have been used in diverse areas, such as radio astronomy, nuclear magnetic resonance, electron spin resonance, and control of gas absorption stabilized lasers [3]. However, current commercial LIAs, which are expensive, heavy, and power-hungry, are not considered suitable for use in portable sensing systems that utilize single-supply battery cells. However, analysis of PSD principles shows that implementation of "handy" LIAs is possible [5]–[10].

A perusal of literature shows that both analog [7]–[10] and digital [11]–[13] LIAs have been used as measurement devices in sensor applications. Performing PSD operations by digital signal processing techniques is a suitable option only when the processing electronic device includes enough computing power to undertake the mathematical operations needed. On the contrary, for portable sensor applications, which contain embedded low-power microcontrollers with limited computing power, analog LIA is the best solution.

To the best of authors' knowledge, there are no commercial portable analog LIAs. Some commercial integrated circuits, such as demodulators or analog multipliers, e.g., AD630 from Analog Devices, indicate in their datasheet how they can be part of a whole LIA, with appropriate additions [14]. However, their supply voltages and consumption levels are still too high for portable systems. Furthermore, in all the analog LIAs reported so far, the system input is a sinusoidal wave [7]–[10]. However, in microcontrolled systems, a more compact, low-voltage, and low-power solution can be reached by considering, instead of a sinusoidal input wave, a square one that can be obtained directly from the digital output ports of the embedded microcontroller, thus avoiding the need for additional electronic components, such as sinusoidal oscillators or function generators.

The purpose of this paper is to propose, against this background, an algorithm that permits a single-supply dual-phase analog LIA to properly process square waves buried in high noise levels. It must be capable of recovering both amplitude and phase by means of a low-power microcontroller, and hence, its computational implementation must be as simple as possible. The reliability and versatility of the novel algorithm need to be experimentally tested. A preliminary approach to this algorithm has been already advanced by these authors earlier in [5] and [6]. This paper offers an in-depth development of the dual PSD technique for processing of square signals, showing recovery equations for both amplitude and phase. Furthermore, the exhaustive experimental verification carried out here improves the previously presented results.

Manuscript received July 8, 2013; revised October 7, 2013; accepted December 13, 2013. Date of publication January 15, 2014; date of current version May 2, 2014. This work was supported in part by the Ministry of Economy and Competitiveness–Fons Europeu de Desenvolupament Regional (MINECO-FEDER) under Grant RYC-2008-03185 and Grant TEC2012-30802, and in part by FPU Fellowship under Grant FPU12/03869.

The authors are with the Group of Electronic Design, Aragon Institute of Engineering Research (GDE-I3A), University of Zaragoza, 50009 Zaragoza, Spain (e-mail: jag@unizar.es; dgromeo@unizar.es; nmedrano@unizar.es; becalvo@unizar.es; scelma@unizar.es).

Color versions of one or more of the figures in this paper are available online at http://ieeexplore.ieee.org.

Digital Object Identifier 10.1109/TIE.2014.2300054

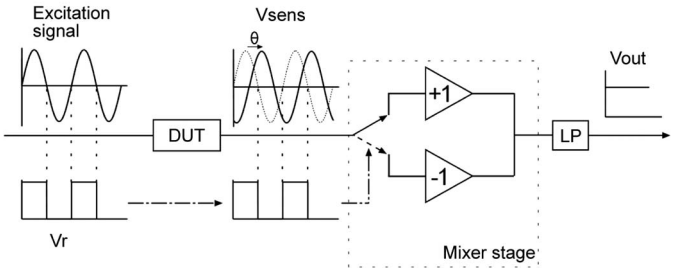

Fig. 1. Block diagram of an analog PSD system, consisting of a mixer and an LP filter.

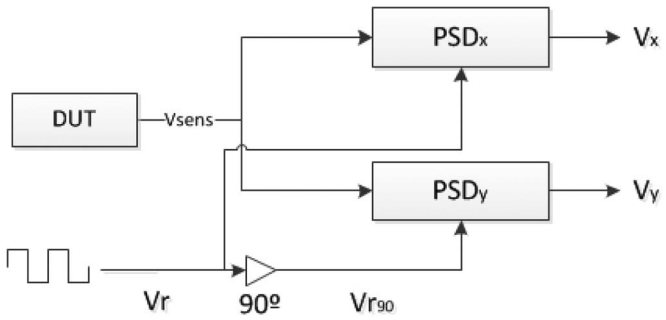

Fig. 2. Block diagram of a dual-branch LIA.

The remainder of the paper is organized as follows. Section II presents the PSD technique, adapted to work in single-supply mode. Section III describes in detail the new proposed algorithm, which allows processing and recovering information from square input signals. Section IV describes the design, implementation, and characterization of a prototype using commercial off-the-shelf components. Section V summarizes the conclusions of this paper.

II. PSD Technique

The simplest way to implement PSD technique [3] is shown in Fig. 1. Typically, a device under test (DUT), i.e., normally a sensor, is excited by a sinusoidal signal of known frequency ω provided by an oscillator or function generator. The DUT generates an output signal, with the same frequency ω and arbitrary amplitude A_S and phase shift θ, i.e., $V_{\rm sens}(t) = A_S \sin(\omega t + \theta)$. This signal enters the mixer stage, where it is multiplied either by 1 or -1, according to the value of a square reference signal V_r having the same frequency and phase as those of the excitation signal. The mixer output is a phase-sensitive rectified version of signal $V_{\rm sens}$. Then, by using a low-pass (LP) filter, noise coupled at frequencies different than ω is canceled, and the $V_{\rm sens}$ signal amplitude A_S extracted according to [2]

$$V_{\rm out} = \frac{2A_S \cos(\theta)}{\pi}. \tag{1}$$

This scheme does not provide any means to calculate the phase shift θ; hence, it is suitable just for systems that do not shift the phase of their excitation signal. Even in those cases, condition $\theta = 0$ is difficult to ensure; thus, for reliable LIA implementations, additional phase-shift controller circuitry should be included to have these signals in-phase.

This limitation can be solved by using, instead of a single branch, a dual LIA, which includes a second PSD system (see Fig. 2). Both branches are controlled by two square reference signals having the same frequency and 90° phase shift between them, i.e., V_r and V_{r90} [2]. The dc signals at the outputs of both X- and Y-branches are given by

$$V_X = \frac{2A_S \cos(\theta)}{\pi} \tag{2}$$

$$V_Y = \frac{2A_S \sin(\theta)}{\pi}. \tag{3}$$

Thus, although the phase shift θ changes, it is possible to recover both the signal amplitude and phase shift generated by the DUT according to

$$A_S = \frac{\pi}{2}\sqrt{V_X^2 + V_Y^2} \tag{4}$$

$$\theta = \arctan(V_Y/V_X). \tag{5}$$

Therefore, the LIA scheme considered in this paper consists of two parallel PSD branches, thus allowing the lock-in's use for sensors that can introduce phase shift. The conceptual scheme of the processing system is shown in Fig. 3(a). If one considers a single supply biasing from 0 to V_{DD}, a quadrature sinusoidal oscillator (or an equivalent stage) generates two signals, which by means of comparators, become 0-V_{DD} square ones used as reference signals V_r and V_{r90} for the two lock-in branches. One of the sinusoidal signals provided by the oscillator is also used as the excitation DUT signal. The DUT output, plus a common-mode voltage V_C added to keep the signal within the supply range, is now given by

$$V_{\rm sens} = V_C + A_S \sin(\omega t + \theta). \tag{6}$$

The mixer, which forms the core block of the LIA, has to be designed considering that it has to operate in single-supply mode. Fig. 3(b) shows the proposed mixer stage. It is basically a differential amplifier whose inputs are switched according to the value of V_r (or V_{r90}) so that its operation is given by

$$V_{0X,0Y} = \begin{cases} (V_{DD} - V_{\rm sens}), & \text{if } V_{r,r90} = V_{DD} \\ (V_{\rm sens} - 0V), & \text{if } V_{r,r90} = 0. \end{cases} \tag{7}$$

Thus, the dc voltages V_X and V_Y at the outputs of both LIA branches are given by [15]

$$V_X = \frac{V_{DD}}{2} - \frac{2A_S \cos(\theta)}{\pi} \tag{8}$$

$$V_Y = \frac{V_{DD}}{2} - \frac{2A_S \sin(\theta)}{\pi}. \tag{9}$$

These equations depend only on the sensor signal amplitude and phase shift, and not on the mode voltage V_C. From (8) and (9), it is possible to obtain the sensor signal amplitude A_S and phase θ as functions of V_X and V_Y

$$A_S = \frac{\pi}{2}\sqrt{\left(V_X - \frac{V_{DD}}{2}\right)^2 + \left(V_Y - \frac{V_{DD}}{2}\right)^2} \tag{10}$$

$$\theta = \arctan\left(V_Y - \frac{V_{DD}}{2} \Big/ V_X - \frac{V_{DD}}{2}\right). \tag{11}$$

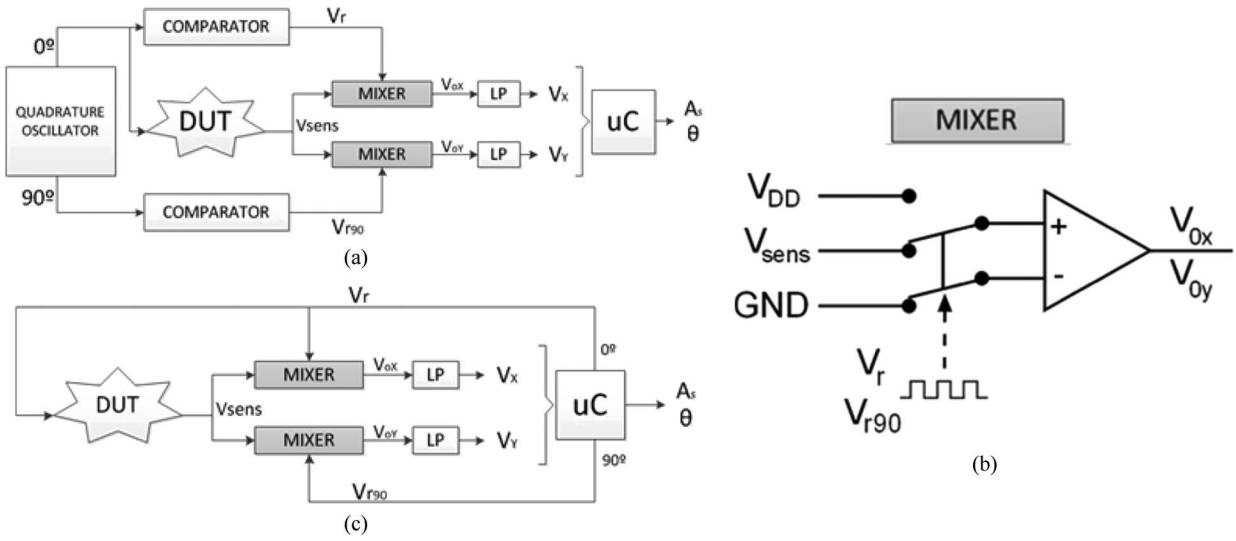

Fig. 3. Block scheme of a single-supply LIA for processing (a) sinusoidal and (c) square input signal. (b) Mixer stage adapted to work in single-supply operation.

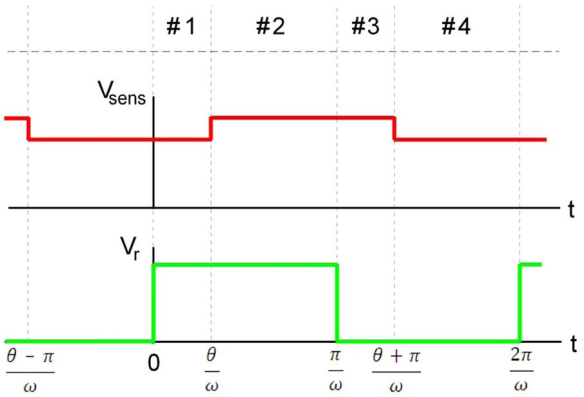

Fig. 4. DUT signal V_{sens} and reference signal V_r waveforms.

In microcontrolled systems, the microcontroller itself can act as an accurate wave generator, providing not sinusoidal but square excitation and reference signals. Based on this approach, the proposed LIA block scheme is shown in Fig. 3(c). The microcontroller acts as a square-wave generator providing two 0–V_{DD} quadrature square waves V_r and V_{r90}, which are used as reference inputs for the two lock-in branches. The first reference signal is, in addition, used as the signal for exciting the sensor. The main advantages of this configuration are size and power reduction due to removability of quadrature oscillator and comparators, as well as ease of programming and design simplicity. On the other hand, (10) and (11) are not valid; hence, a new algorithm to process PSD square signals must be developed.

III. Proposed Algorithm

Some previous works [2]–[4] have proposed techniques to recover information using LIAs processing square signals. However, none of them could offer a complete solution for accurate recovery of amplitude and phase.

The novel algorithm described in this paper allows obtaining the expressions of the lock-in outputs, i.e., V_X and V_Y, by analyzing how both the mixer stage and the LP filter process square sensor signals. Fig. 4 illustrates the evolution in time

TABLE I
Mixer Operation Modes (V_X Branch, One V_r Period)

Case	V_{sens}	V_r	Duration time	V_{sens}	Mixer Output (V_{oX})
#1	L	H	$\frac{\theta}{\omega}$	$V_C - A_S$	$V_{DD} - V_{SENS}$
#2	H	H	$\frac{\pi-\theta}{\omega}$	$V_C + A_S$	$V_{DD} - V_{SENS}$
#3	H	L	$\frac{\theta}{\omega}$	$V_C + A_S$	V_{SENS}
#4	L	L	$\frac{\pi-\theta}{\omega}$	$V_C - A_S$	V_{SENS}

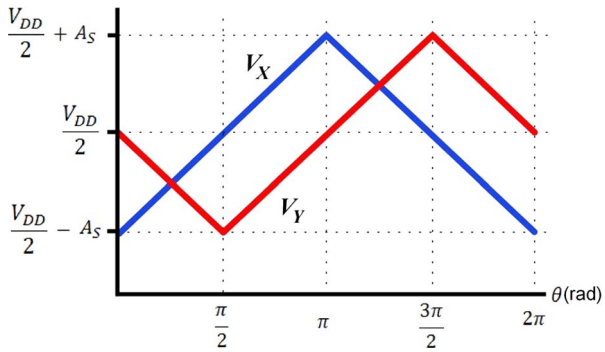

Fig. 5. Output signals V_X and V_Y as a function of phase shift θ for square input signal.

of the square DUT signal V_{sens} and the X-branch control signal V_r. Depending on the DUT-to-reference phase shift θ, the DUT output signal can be expressed as an alternate succession of discrete voltage levels $V_C \pm A_S$, where V_C is again the common-mode voltage and A_S is the sensor signal amplitude

$$V_{\text{sens}} = \begin{cases} (V_C - A_S), & \text{if } \frac{\theta-\pi}{\omega} < t < \frac{\theta}{\omega} \\ (V_C + A_S), & \text{if } \frac{\theta}{\omega} < t < \frac{\theta+\pi}{\omega}. \end{cases} \quad (12)$$

Assuming V_{sens} and V_r as two periodic bivalued signals, the X-branch mixer operation encloses four cases depending on the high/low levels for V_{sens} and V_r, which result in four different values at the mixer output, as summarized in Table I.

TABLE II
RECOVERY VALUES FOR BOTH AMPLITUDE A_S AND PHASE θ

$\mathbf{V_X}$	$< \frac{V_{DD}}{2}$	$> \frac{V_{DD}}{2}$	$> \frac{V_{DD}}{2}$	$< \frac{V_{DD}}{2}$
$\mathbf{V_Y}$	$< \frac{V_{DD}}{2}$	$< \frac{V_{DD}}{2}$	$> \frac{V_{DD}}{2}$	$> \frac{V_{DD}}{2}$
$\mathbf{A_S}$	$V_{DD} - V_X - V_Y$	$V_X - V_Y$	$V_X + V_Y - V_{DD}$	$V_Y - V_X$
$\boldsymbol{\theta}$	$\left(\frac{V_Y - \frac{V_{DD}}{2}}{V_X + V_Y - V_{DD}}\right)\frac{\pi}{2}$ $\in \left[0, \frac{\pi}{2}\right]$	$\pi + \left(\frac{V_Y - \frac{V_{DD}}{2}}{V_X - V_Y}\right)\frac{\pi}{2}$ $\in \left[\frac{\pi}{2}, \pi\right]$	$\pi + \left(\frac{V_Y - \frac{V_{DD}}{2}}{V_X + V_Y - V_{DD}}\right)\frac{\pi}{2}$ $\in \left[\pi, \frac{3\pi}{2}\right]$	$2\pi - \left(\frac{V_Y - \frac{V_{DD}}{2}}{V_Y - V_X}\right)\frac{\pi}{2}$ $\in \left[\frac{3\pi}{2}, 2\pi\right]$

Thus, V_X can be calculated as the average value over a period of signal V_r of the four cases obtained at the output of the mixer stage presented in Table I, i.e.,

$$\begin{aligned} V_X = \frac{\omega}{2\pi}\Bigg\{ & \left(\frac{\theta}{\omega}\right)\cdot[V_{DD} - (V_C - A_S)] \\ & + \left(\frac{\pi-\theta}{\omega}\right)\cdot[V_{DD} - (V_C + A_S)] \\ & + \left(\frac{\theta}{\omega}\right)\cdot[V_C + A_S] + \left(\frac{\pi-\theta}{\omega}\right)\cdot[V_C - A_S]\Bigg\} \\ = & \frac{V_{DD}}{2} - A_S + \frac{2A_S}{\pi}\theta. \end{aligned} \tag{13}$$

Because of V_{sens} discontinuities, (13) is defined only in a closed domain $[0, \pi]$ of the θ variable. To generalize it for any θ value within the $[0, 2\pi]$ range, symmetry properties of cosine functions can be applied, obtaining the following expression:

$$V_X = \frac{V_{DD}}{2} - A_S + \frac{2A_S}{\pi}\arccos\left(\cos(\theta)\right). \tag{14}$$

For the Y-branch, output V_Y can be similarly calculated. Assuming that its control signal V_{r90} is $\pi/2$ shifted from V_r, then the phase shift between V_{sens} and V_{r90} is $\theta - \pi/2$. Thus, V_Y is given by

$$\begin{aligned} V_Y &= \frac{V_{DD}}{2} - A_S + \frac{2A_S}{\pi}\arccos\left(\cos\left(\theta - \frac{\pi}{2}\right)\right) \\ &= \frac{V_{DD}}{2} - A_S + \frac{2A_S}{\pi}\arccos\left(\sin(\theta)\right). \end{aligned} \tag{15}$$

From the analyzed results, it is worth noting that, when using a sinusoidal excitation, the equations to recover V_X and V_Y are smooth functions [see (8) and (9)]. However, for signals of square-wave excitation, the corresponding recovery expressions (14) and (15) are piecewise functions of the phase shift θ, as shown in Fig. 5. Thus, it is possible to get their values over the full $[0, 2\pi]$ range by applying the corresponding piecewise linear expressions

$$V_X = \begin{cases} \left(\frac{V_{DD}}{2} + \frac{2A_S}{\pi}\theta - A_S\right), & \text{if } 0 < \theta < \pi \\ \left(\frac{V_{DD}}{2} - \frac{2A_S}{\pi}\theta + 3A_S\right), & \text{if } \pi < \theta < 2\pi \end{cases} \tag{16}$$

$$V_Y = \begin{cases} \left(\frac{V_{DD}}{2} - \frac{2A_S}{\pi}\theta\right), & \text{if } 0 < \theta < \pi/2 \\ \left(\frac{V_{DD}}{2} + \frac{2A_S}{\pi}\theta - 2A_S\right), & \text{if } \frac{\pi}{2} < \theta < \frac{3\pi}{2} \\ \left(\frac{V_{DD}}{2} - \frac{2A_S}{\pi}\theta + 4A_S\right), & \text{if } \frac{3\pi}{2} < \theta < 2\pi. \end{cases} \tag{17}$$

To sum up, by analyzing (16), (17), and Fig. 5, it becomes clear that the method suitable for recovering DUT signal parameters A_S and θ consists in dividing the full θ interval $[0, 2\pi]$ into four subintervals, each of $\pi/2$ size (separated in Fig. 5 by vertical dotted lines), and selecting the suitable V_X and V_Y expression in each case. The system finds out the correct subinterval by comparing the relative values of V_X and V_Y with respect to $V_{DD}/2$, according to Table II. These output expressions depend on the same variables as those in the sinusoidal case, i.e., the signal amplitude A_S and the phase shift θ introduced by the DUT. A remarkable feature of these expressions is that, again, there is no dependence on the common mode V_C.

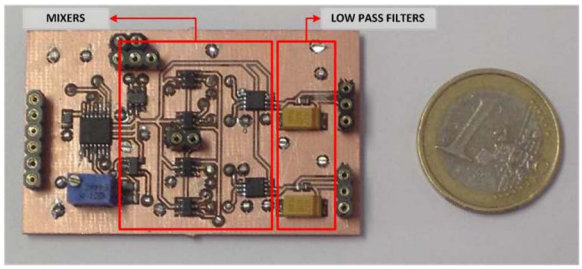

Fig. 6. Photograph of the LIA prototype (53 mm × 32 mm).

Note that the just described system operation can remind to a phase detector within a phase-locked loop (PLL) [16]. However, the goal of a phase detector in a PLL is to compare the phase between two signals, whereas the proposed system looks for an accurate measurement of both the phase and amplitude of the DUT output signal.

IV. EXPERIMENTAL VERIFICATION

A. Hardware Implementation

To validate this algorithm, an analog low-voltage single-supply LIA has been implemented using low-voltage low-power compliant commercial components. A voltage level of 3.3 V has been selected for powering up the devices as a typical bias voltage in portable sensing systems.

The designed LIA (see Fig. 6) consists of a double mixer stage, X and Y, followed by two LP filters, respectively, providing the dc signals V_X and V_Y that are needed for obtaining A_S and θ. Each mixer is composed of two ADG719 2:1 multiplexers from Analog Devices and a unity gain differential amplifier AD8476 from Analog Devices. Finally, each LP filter is a passive RC circuit with a cutoff frequency in the hertz range.

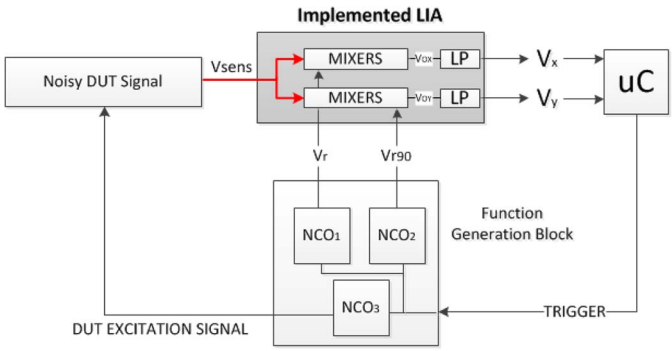

Fig. 7. Block diagram of the experimental setup.

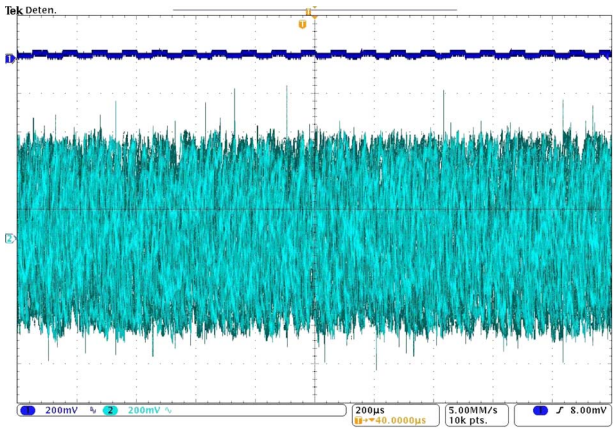

Fig. 8. V_{sens} for a noise level of (top) null amplitude and (bottom) noise amplitude value of 500 mV.

Fig. 7 shows the experimental setup block diagram. Input signal V_{sens} is a noisy square-wave signal centered on a dc level V_C. This dc level places the signal between supply levels, for a proper function of the commercial components, while noise amplitude can be modified. For accurate control of the LIA working conditions during the test, all the control signals of the system are created in a function generation block. This block provides two square-wave signals in quadrature (V_r, V_{r90}) at the same frequency, used as control signals, plus an additional square signal that is used to excite the DUT. These three square waves are generated by AD9834 numerically controlled oscillators (NCOs) from Analog Devices, using a 10-MHz quartz crystal as a reference for signal generation. The NCOs are connected to a microcontroller by SPI [17], and all of them are triggered with the same signal provided by the microcontroller, which consequently allows control phase shift between them. The desired phase in the V_{sens} signal is thus selected by properly triggering the corresponding NCO.

Fig. 8 shows V_{sens} in the presence of two different noise levels. The signal on top is V_{sens} with a noise level of null amplitude, whereas the one on the bottom illustrates noise amplitude fifty times higher than the ideal data signal amplitude. Figs. 9 and 10 show the waveforms obtained throughout the LIA. Fig. 9(a) and (b) shows the outputs of multiplexers, i.e., switched between GND and $V_{\text{sens}}(V_{0LX,0LY})$ and between V_{sens} and $V_{DD}(V_{0HX,0HY})$, also of the differential amplifiers V_{0X} and V_{0Y}. Fig. 10 provides the dc outputs V_X and V_Y from the mixer signals V_{0X} and V_{0Y}.

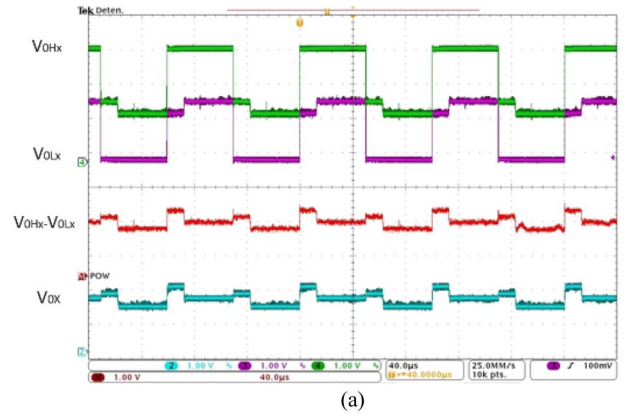

Fig. 9. Outputs of the multiplexers. $(V_{0HX}, V_{0LX}, V_{0HY}, V_{0LY})$. Theoretical V_{0X} and V_{0Y} signals $(V_{0HX} - V_{0LX}, V_{0HY} - V_{0LY})$. Experimental V_{0X} and V_{0Y}. (a) X-branch. (b) Y-branch.

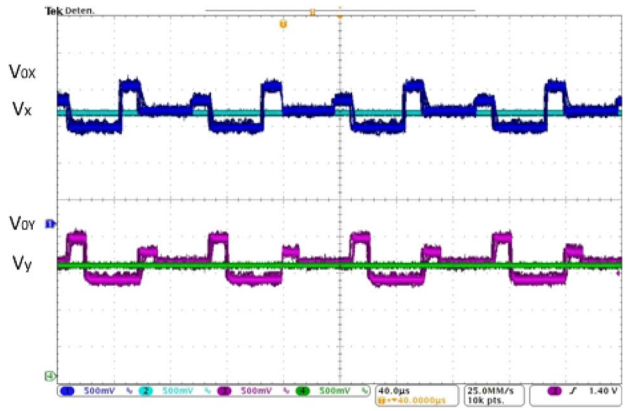

Fig. 10. LP filter inputs (V_{0X}, V_{0Y}) and outputs V_X, V_Y.

TABLE III
TEST SIGNALS' CHARACTERISTICS

Signal name	Frequency	Amplitude
A	10 kHz	9 mV
B	76 kHz	22 mV

To avoid losing information, both V_X and V_Y have to be precisely digitized. Several tests were carried out by using different ADC resolutions from 8 to 24 bits. As expected, higher number of bits allows reading smaller variations in the target signal. The results shown in Figs. 12–14 were obtained by using 18-bit digitization provided by two 24-bit LTC2400 ADCs from

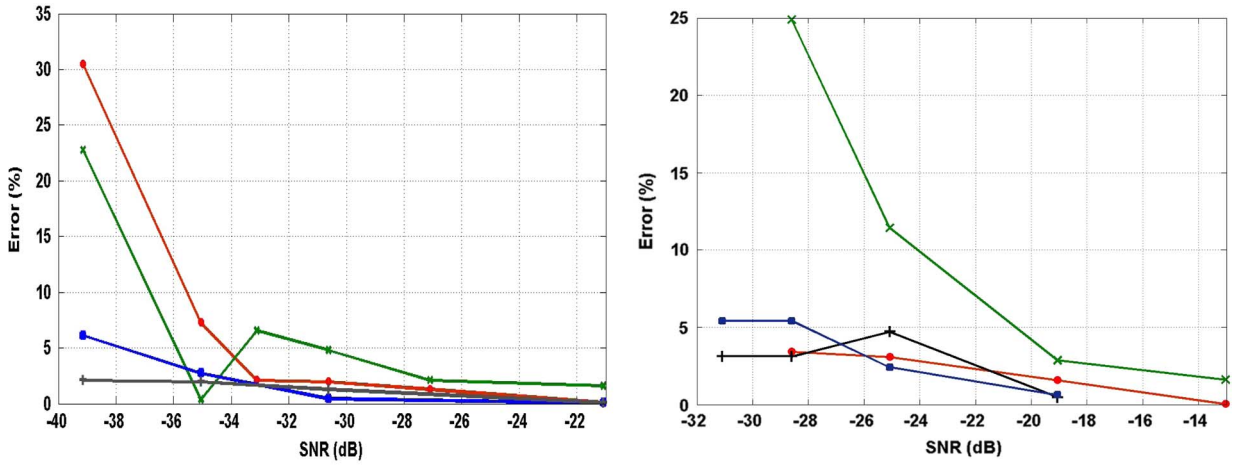

Fig. 11. Error in both phase and amplitude recovery for (a) signal A and (b) signal B buried in noise. Markers: (x) Phase error with white noise, (□) amplitude error with white noise, (●) phase error with flicker noise, and (+) amplitude error with flicker noise.

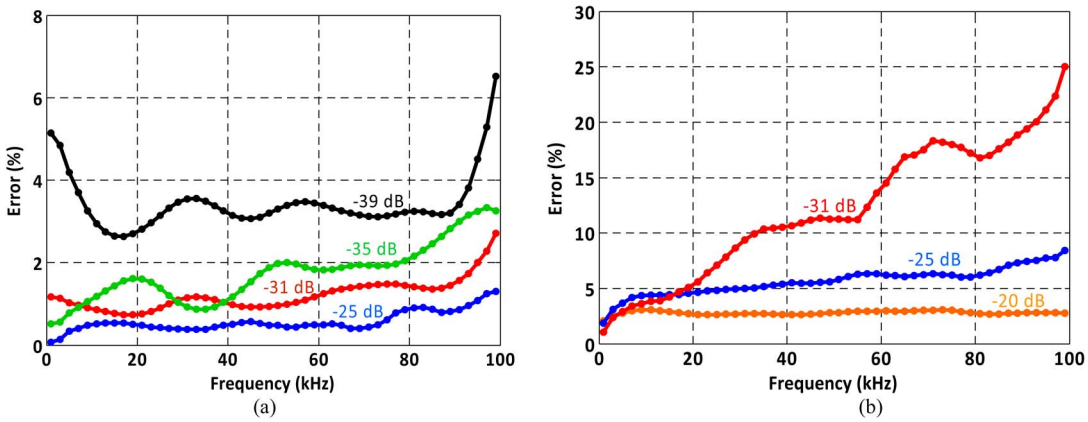

Fig. 12. Error in (a) amplitude and (b) phase recovery as a functions of the frequency for different SNR levels. In all cases, $A_s = 22$ mV.

Linear Technology. With 18 effective bits of resolution over a power supply voltage reference of 3.3 V, the algorithm is sensitive enough to read out signals of tens of microvolts.

B. Experimental Results

The performance of the designed analog LIA in recovering information from signals buried in high noise levels has been evaluated with controllable noise levels. Two different noise-free square signals denoted hereafter as signals A and B have been utilized. Table III presents their characteristics, which are in the same range as that of the previously reported analog LIAs working with sinusoidal inputs [7]–[10]. Both signals allow the application of the proposed algorithm with a great number of sensors, which work at frequencies of tens of kilohertz giving very noisy output signals.

1) White and Flicker Noise Tests: First, the system has been tested using signals buried in both white noise [18], [19] and flicker noise [19], [20]. Flicker noise was generated using a USB6212 data acquisition (DAQ) board from National Instruments, with a corner frequency of 100 kHz; white noise was generated using a 33522A function wave generator from Agilent Technologies, with a noise bandwidth of 100 MHz. Noise levels are defined using the signal-to-noise ratio (SNR), given by the following equation:

$$\text{SNR} = 20 \cdot \log_{10} \frac{A_S}{A_{\text{NOISE}}}. \tag{18}$$

Error levels achieved in recovering signal amplitude and phase at different conditions and noise types are shown in Fig. 11. Fig. 11(a) shows the errors for both types of noise versus different SNR levels for signal A. In this case, error remains below 5% for SNR levels down to -30 dB. Fig. 11(b) shows the corresponding results for signal B. In this case, the error remains below 5% for SNR levels down to -20 dB.

Furthermore, Fig. 12 shows the signal recovery error versus operating frequency. The frequency ranges from 1 to 99 kHz in 2-kHz steps, and measurements correspond to a signal amplitude of 22 mV buried in different white noise with SNR levels up to -39 dB. As shown, amplitude error [see Fig. 12(a)] remains below 7% in all cases, whereas phase recovery [see Fig. 12(b)] is more frequency dependent and less tolerant to noise, providing an error below 8% for SNR $= -25$ dB over all the frequency range.

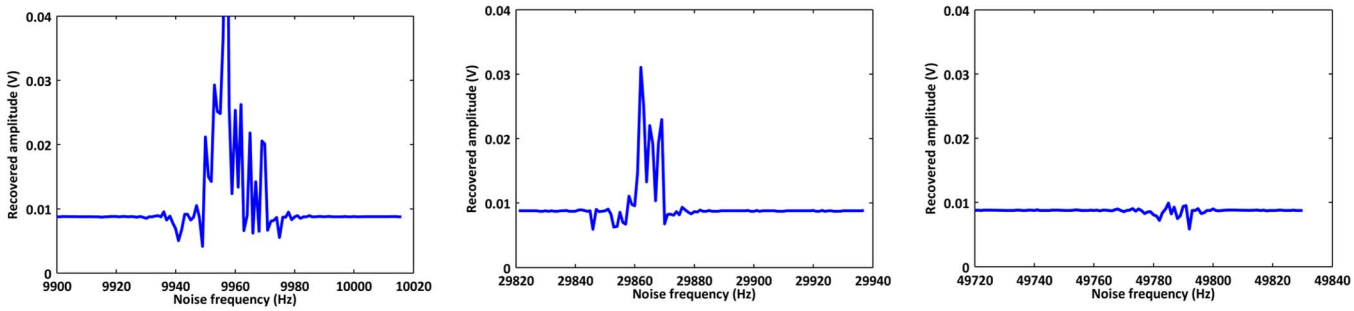

Fig. 13. Amplitude recovery for signal A buried in 100-mV-amplitude sinusoidal interference whose frequency is around the main frequency components of the square data signal: (a) first harmonic, (b) third harmonic, and (c) fifth harmonic.

TABLE IV
INTERFERENCE TEST RESULTS

Signal	Harmonic	MAx. in-band error (%)	Dead band span (Hz)
A	First	>100	40
	Third	>100	40
	Fifth	20	30
B	First	52	40
	Third	5	5
	Fifth	1	-

2) Interference Tests: The other typical signal perturbation is interference, which has been provided by the DAQ board. For single harmonic data signals (e.g., sinusoidal), when noise frequency differs from that of data signal, noise can be completely rejected, as mentioned in Section II. For a square data signal, formed by a main frequency plus the contribution of successive odd harmonics, the results obtained by adding sinusoidal interference noise frequencies show that error is negligible in the spectrum as a whole, except for interference frequencies close to the first harmonics. Experimentally, for operation frequencies up to around 40 kHz, the number of harmonics presenting a dead band (i.e., a frequency span in which error is higher than 2%) is three, whereas for frequencies from 40 to 100 kHz, the interference affects only the two first harmonics and the effects in the fifth harmonic are negligible.

Fig. 13(a)–(c) shows the amplitude recovered when sensor signal A has interference that concurs with the first [see Fig. 13(a)], third [see Fig. 13(b)], and fifth [see Fig. 13(c)] harmonics. It is shown that there is a maximum dead band of 40 Hz around these harmonics where the error drastically increases. A more exhaustive analysis shows that dead band span remains below 40 Hz for signal frequencies from 1 to 100 kHz. Table IV presents the effects of harmonic interference for signals A and B.

C. Practical Applications

Experimental results have been obtained assuming a perfect square signal buried in noise as a response of a sensor, which can be realistic in certain applications, such as acoustic or optical sensors [21] However, in applications such as capacitive or resonant sensors where more specific solutions can be found [22], the sensor itself distorts the square wave, thus reducing the chance of accurate recovery of the output signal amplitude. However, the usual goal of such applications is to obtain the resonance frequency, which can be done by performing a frequency sweep and phase tracking [23], [24]. Therefore, despite the error in amplitude recovery being high in such cases, the algorithm can carry out phase measurements accurately, thus obtaining the resonance frequency, as shown in [25]. To support this statement, Fig. 14 shows phase tracking in a frequency sweep for a resonant RLC configuration excited by a square-wave signal and compares the results to the measurements obtained with the classical sine approach and with a commercial DSP LIA 7265 from Signal Recovery. The maximum slope in all the curves [see Fig. 14(a)] matches at the same frequency [see Fig. 14(b)], which is the resonance frequency.

V. CONCLUSION

This paper has presented an algorithm that can accurately recover amplitude and phase from square signals buried in high noise levels, by means of an analog dual-phase LIA.

First, theoretical estimation has been explained in detail, starting with the classical PSD techniques using sinusoidal signal and justifying the need for a new algorithm that can process square signals. Second, the proposed algorithm has been picked apart in every possible scenario, providing the reader with a detailed explanation on how the recovery works.

An exhaustive experimental verification has been done, accurately controlling the test conditions by means of an external signal generation block. Results validate that the proposed algorithm can recover low signals down to 9-mV amplitude and 10-kHz frequency buried in -30-dB noise levels with less than 5% error. It is also shown that frequencies up to 76 kHz and 22-mV-amplitude signals buried in -20-dB noise levels can be recovered with less than 5% error.

Use of square signals for exciting sensor reduces size and power consumption because microcontroller can act as a square-wave generator. Moreover, it also improves versatility and computational simplicity of the detection system. These features allow the implementation of a low-power LIA similar to the one described in Section IV in a portable sensing system, such as an intelligent node of a wireless sensor network or a distributed control system, using it in combination of a wide range of sensors.

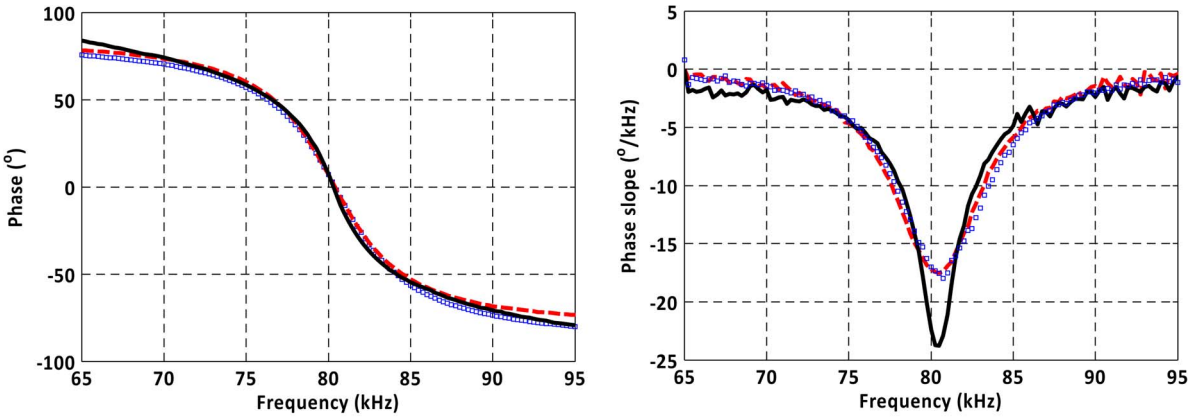

Fig. 14. (a) Phase measurements and (b) slope calculations using (dash) classical algorithm, (square markers) commercial LIA, and (solid) proposed algorithm.

REFERENCES

[1] M. L. Meade, *Lock-in Amplifiers: Principles and Applications.* Stevenage, U.K.: Peregrinus, 1983.

[2] *Lock-In Amplifiers, Appl. Notes*, Stanford Res. Sys., Sunnyvale, CA, USA, 1999, data sheets.

[3] D. P. Blair, "Phase sensitive detection as a means to recover signals buried in noise," *J. Phys E, Sci. Instrum.*, vol. 8, no. 8, pp. 621–627, 1975.

[4] J. H. Scofield, "Frequency-domain description of a lock-in amplifier," *Amer. J. Phys.*, vol. 62, no. 2, pp. 129–133, Feb. 1994.

[5] J. Aguirre, N. Medrano, B. Calvo, and S. Celma, "Lock-in amplifier for portable sensing systems," *Electron. Lett.*, vol. 47, no. 21, pp. 1172–1173, Oct. 2011.

[6] J. Aguirre, N. Medrano, B. Calvo, and S. Celma, "Lock-in amplifier for portable sensing systems," in *Proc. IEEE Sensors*, 2011, pp. 1866–1869.

[7] M. Theodor, U. Karakas, D. Ruh, H. Zappe, and A. Seifert, "Lock-in amplification for implantable multiwavelength pulse oximeters," in *Proc. IEEE Annu. Eng. Med. Biol. Soc.*, 2013, pp. 495–498.

[8] J. Xu, G. Meynants, and P. Merken, "Low-power lock-in amplifier for complex impedance measurement," in *Proc. 3rd Int. Workshop Adv. Sens. Interfaces*, 2009, pp. 110–114.

[9] A. D'Amico, A. De Marcellis, C. Di Carlo, C. Di Natale, G. Ferri, E. Martinelli, R. Paolesse, and V. Stornelli, "Low-voltage low-power integrated analog lock-in amplifier for gas sensor applications," *Sens. Actuators B, Chem.*, vol. 144, no. 2, pp. 400–406, Feb. 2010.

[10] A. De Marcellis, G. Ferri, A. D'Amico, C. Di Natale, and E. Martinelli, "A fully-analog lock-in amplifier with automatic phase alignment for accurate measurements of ppb gas concentrations," *IEEE Sensors J.*, vol. 12, no. 5, pp. 1377–1383, May 2012.

[11] J. Leis, P. Martin, and D. Buttsworth, "Simplified digital lock-in amplifier algorithm," *Electron. Lett.*, vol. 48, no. 5, pp. 259–261, Mar. 2012.

[12] M. Ordonez, M. O. Sonnaillon, J. E. Quaioe, and M. T. Iqbal, "An embedded frequency response analyzer for fuel cell monitoring and characterization," *IEEE Trans. Ind. Electron.*, vol. 57, no. 6, pp. 1925–1934, Jun. 2010.

[13] B. Akin, U. Orguner, H. A. Toliyat, and M. Rayner, "Phase-sensitive detection on motor fault signatures in the presence of noise," *IEEE Trans. Ind. Electron.*, vol. 55, no. 6, pp. 2539–2550, Jun. 2008.

[14] L. Rovati and S. Cattini, "Zero-field readout electronics for planar fluxgate sensors without compensation coil," *IEEE Trans. Ind. Electron.*, vol. 59, no. 1, pp. 571–578, Jan. 2012.

[15] M. Gabal, N. Medrano, B. Calvo, P. Martinez, S. Celma, and M. Valero, "A complete low voltage analog lock-in amplifier to recover sensor signals buried in noise for embedded applications," in *Proc. 24th Eurosensors*, 2010, pp. 74–77.

[16] C. Tang and Q. Xue, "An array of coherent sources based on novel dual-loop PLL infrastructure," *IEEE Trans. Ind. Electron.*, vol. 60, no. 11, pp. 5337–5347, Nov. 2013.

[17] *SPI Block Guide V03.06*, Freescale Semiconductor, Austin, TX, USA, 2000.

[18] P. K. Dash and S. Hasan, "A fast recursive algorithm for the estimation of frequency, amplitude, and phase of noisy sinusoid," *IEEE Trans. Ind. Electron.*, vol. 58, no. 10, pp. 4847–4856, Oct. 2011.

[19] P. R. Gray, P. J. Hurst, S. H. Lewis, and R. G. Meyer, *Analysis and Design of Analog Integrated Circuits,* 4th ed. Hoboken, NJ, USA: Wiley, 2001.

[20] M. R. Nabavi and S. Nihtianov, "Eddy-current sensor interface for advanced industrial applications," *IEEE Trans. Ind. Electron.*, vol. 58, no. 9, pp. 4414–4423, Sep. 2011.

[21] D. W. Sukow, T. Gilfillan, B. Pope, M. S. Torre, A. Gavrielides, and C. Masoller, "Square-wave switching in vertical-cavity surface-emitting lasers with polarization-rotated optical feedback: Experiments and simulations," *Phys. Rev.*, vol. 86, no. 3, pp. 033818-1–033818-8, 2012.

[22] F. Reverter and O. Casas, "A microcontroller-based interface circuit for lossy capacitive sensors," *Meas. Sci. Technol.*, vol. 21, pp. 065203-1–065203-8, 2010.

[23] F. Wang, C. Zou, and J. Quiao, "Dynamic phase-frequency characteristic of thermosonic wire bonder transducer," in *Proc. ICEPT-HDP*, Shanghai, China, 2008, pp. 819–822.

[24] M. A. Urbiztondo, I. Pellejero, M. Villarroya, J. Sesé, M. P. Pina, I. Dufour, and J. Santamaría, "Zeolite-modified cantilevers for the sensing of nitrotoluene vapors," *Sens. Actuators B, Chem.*, vol. 137, no. 2, pp. 608–616, Apr. 2009.

[25] D. García-Romeo, M. P. Pina, N. Medrano, B. Calvo, J. Sesé, I. Pellejero, and D. Antolín, "Portable low-power electronic interface for gas detection using microcantilevers," in *Proc. IECON*, Vienna, Austria, Nov. 10–13, 2013, pp. 3970–3975.

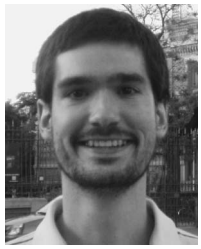

Javier Aguirre received the B.Sc. degree in physics in 2010 from the University of Zaragoza, Zaragoza, Spain, where he is currently working toward the Ph.D. degree in the Group of Electronic Design, Aragon Institute of Engineering Research (GDE-I3A).

His research interests include signal recovery, sensor interfaces, and high-frequency communication circuits.

Daniel García-Romeo received the B.Eng. degree in industrial electronics from the University of Zaragoza, Zaragoza, Spain, where he is currently working toward the Ph.D. degree in the Group of Electronic Design, Aragon Institute of Engineering Research (GDE-I3A).

His research interests include integrated sensor interfaces, signal processing, and intelligent instrumentation.

Nicolás Medrano (M'96) received the B.Sc. and Ph.D. degrees in physics from the University of Zaragoza, Zaragoza, Spain, in 1989 and 1998, respectively.

He is currently an Associate Professor of Electronics with the Faculty of Physics and a Member of the Group of Electronic Design, Aragon Institute of Engineering Research (GDE-I3A), University of Zaragoza. His research interests include implementation of neural networks for signal processing, integrated sensor interfaces, wireless sensor networks, and intelligent instrumentation.

Belén Calvo (M'07) received the B.Sc. degree in physics and the Ph.D. degree in electronics engineering from the University of Zaragoza, Zaragoza, Spain, in 1999 and 2004, respectively.

She is currently a Senior Researcher with the Group of Electronic Design, Aragon Institute of Engineering Research (GDE-I3A), University of Zaragoza. Her research interests include low-voltage low-power analog and mixed-mode CMOS design strategies, implementation and test of reconfigurable smart sensor-to-microcontroller application-specified integrated circuit (ASIC) interfaces, wireless sensors networks, and wideband front-end IC transceivers.

Santiago Celma was born in Zaragoza, Spain. He received the B.Sc., M.Sc., and Ph.D. degrees from the University of Zaragoza, Zaragoza, in 1987, 1989, and 1993, respectively, all in physics.

He is currently a Full Professor with the Group of Electronic Design, Aragon Institute of Engineering Research (GDE-I3A), University of Zaragoza. He has coauthored more than 80 technical papers and 270 international conference contributions. He is a coauthor of three books and the holder of four patents. He appears as Principal Investigator in more than 25 national and international research projects. His research interests include circuit theory, mixed-signal integrated circuits, high-frequency communication circuits, and wireless sensor networks.